2.5 PREPRINT

1988 NHTC. Paper. (NATIONAL HEAT TRANSFER CONF

HOUSTON

3430

HIGH RAYLEIGH NUMBER NATURAL CONVECTION IN PARTIALLY DIVIDED AIR AND WATER FILLED ENCLOSURES

Joel Neymark, Graduate Student*
Allan Kirkpatrick, Associate Professor*
Ren Anderson, Senior Engineer**
Charles Boardman, Graduate Student*

* M.E. Department, Colorado State University, Fort Collins, CO
** Solar Energy Research Institute, Golden, CO

ABSTRACT

In this research experiments were conducted using a representative cubic geometry differentially heated from the side with an internal partial vertical partition. Both air (Pr $\simeq$ 0.7) and water (Pr $\simeq$ 6.0) were used separately as the working fluid. Two test cells, an air cell at Colorado State University and a water cell at SERI were used. The aperture geometry was doorway-like, with the height of the aperture at half of the enclosure height. The aperture width was varied so that the aperture area ratio ranged from 0.003 to 0.5. The flux Rayleigh number varied from about 4×10^{11} to 1×10^{13}. Nusselt-Rayleigh aperture area ratio correlation curves were developed for both the air and the water data. For a constant Rayleigh number, as the aperture area was decreased, the flow field underwent a transition from a boundary layer regime at relative aperture areas above 0.02, to a blocked flow bulk density driven regime, resulting in a significant decrease in the Nusselt number, and increase in the horizontal stratification across the aperture.

NOMENCLATURE

Ap	Dimensionless aperture opening, hw/HW
g	Gravitational acceleration
h	Height of aperture (h = H/2)
H	Height of enclosure
k	Thermal conductivity
Nu	Nusselt number, $q"H/k\Delta T$
Pr	Prandtl number ν/α
Q	Convective heat transfer
q"	Convective heat transfer/area
Ra_*	Rayleigh number, $g\beta H^3\Delta T/\nu\alpha$
Ra^*	Flux Rayleigh number, $g\beta H^4 q"/k\nu\alpha$
T_c	Temperature of isothermal cold wall
T_H^c	Temperature of cold zone at y = H/4
T_c^H	Temperature of hot wall at y = H/2
T_H^H	Temperature of hot zone at y = H/4
$T_{H/2}$	Temperature of hot or cold zone at y = H/2
w	Width of aperture
W	Width of enclosure
α	Thermal diffusivity
β	Coefficient of thermal expansion
ΔT^*	Dimensionless horizontal stratification across aperture, $(T'_H - T'_c)/(T_H - T_c)$
ν	Kinematic viscosity
ϵ	Emissivity
θ	Dimensionless vertical stratification, $(T_y - T_c)/(T_{H/2} - T_c)$

INTRODUCTION

A basic configuration for the study of natural convection in complex enclosures is the partially divided enclosure. In this configuration an enclosure differentially heated from the side is divided into two zones which communicate laterally across an aperture. This type of flow situation arises in a large number of engineering applications including heating and cooling of buildings, fire and smoke spread, indoor air quality, and electronic equipment cooling.

At high flux Rayleigh numbers ($Ra^* > 10^{10}$) thermal transport across an undivided enclosure is in the form of boundary layers which move laterally along the periphery of the enclosure. The temperature field in the core of the enclosure is uniform in the horizontal direction. When the enclosure is partially divided by a partition the flow is redirected through the interior core. The resulting transport across the aperture can be driven not only by active wall boundary layers, but also by the bulk density difference resulting from the development of the horizontal stratification across the aperture.

A review of natural convection in buildings, including partially divided enclosures is given in Anderson and Kreith (1987). Natural convection through apertures has traditionally been studied by either 1) correlating the transport through the aperture with the fluid conditions on either side of the aperture, or 2) correlating the transport through the aperture with the far wall boundary conditions. Brown and Solvason (1962) developed an aperture flow model for enclosures with horizontal or vertical partitions, and correlated

the aperture transport with the fluid conditions on either side of the aperture. High Rayleigh number natural convection heat transfer measurements have been reported by Nansteel and Greif (1984) for a water filled enclosure of aspect ratio 0.5 with both two- and three-dimensional vertical partitions and wall to wall Rayleigh numbers between 10^9 and 10^{11}. The three-dimensional aperture width relative to the enclosure width was held constant at 0.093, and the aperture height varied from 1/4 to 1 of the enclosure height, so for a half height aperture, the aperture ratio was 0.047. Nusselt-Rayleigh number data for a water-filled partially divided enclosure of aspect ratio 0.3 with a single two-dimensional partition have been correlated by Lin and Bejan (1983) for Rayleigh numbers between 10^9 and 10^{10}. Both of these studies demonstrated that the heat transfer above the top of the aperture in the hot zone is significantly reduced in the presence of an aperture due to flow separation along the active wall. The flow field was found to be laminar along the heated and cooled walls.

Natural convection experiments in air at high Rayleigh number are primarily limited to unpartitioned enclosures. A flow visualization experiment by Olson, Glicksman and Ferm (1986) in a full-scale enclosure at $Ra = 2 \times 10^{10}$ indicated that the boundary layer flow on the heated and cooled walls was turbulent. Turbulent temperature profiles at high Rayleigh number have been measured by Cheesewright and Zial (1986). Recently, attempts have been made to couple the aperture region to the wall region boundary conditions. Scott, Anderson, and Figliola (1986) suggested that the temperature difference across the aperture was controlled by the possible blockage of the wall boundary layers by the opening aperture. They consequently found that, for water as the heat transfer fluid, the temperature difference across the aperture rose sharply when the nondimensional aperture area was reduced to below 2 percent of the heated wall area.

The majority of the partially divided enclosure experiments have been conducted using water ($3 < Pr < 7$) as the working fluid. Experimental data for air-filled partially divided enclosures is lacking. Specifically, the effect of the aperture on the boundary layer flow at the active wall surfaces is unknown.

The objective of this paper is to experimentally determine the flow and heat transfer characteristics of air- and water-filled partially divided enclosures at high flux Rayleigh numbers. Specific goals are to: determine under what conditions an enclosure will become horizontally stratified, and the resulting effect on the cross cavity Nusselt number, and to compare the behavior of small-scale water models with full-scale air enclosures.

The representative geometry studied is shown in Figure 1. It is a cube with a vertical partition in the center. The partition aperture is of a doorway geometry, with height h fixed at one-half the enclosure height H, and variable width w. The nondimensional aperture ratio, Ap, is defined as the ratio of the doorway area to the heated wall area. The thermal boundary conditions were chosen to be representative of conditions in a building interior: a constant heat flux hot wall, and a constant temperature cold wall. The other surfaces are considered to be adiabatic. Similarity between two natural convection experiments require matching Ra^*, Pr, geometry, and the thermal boundary conditions of the interior surfaces. Rayleigh number similarity between air and water experiments can be achieved by appropriate choice of length scale and temperature difference. It is not possible to match Prandtl numbers of air and water.

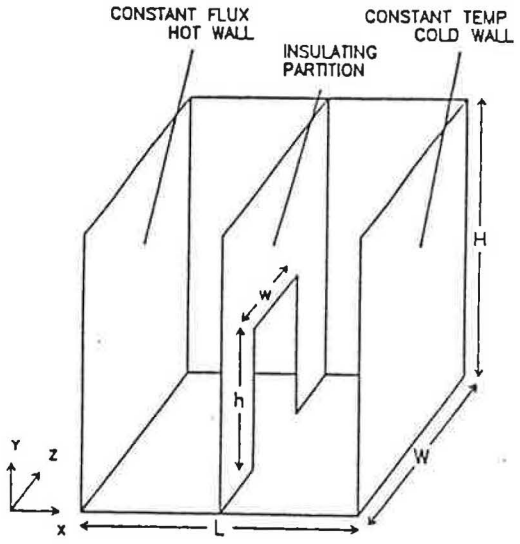

Figure 1. Representative geometry.

DESCRIPTION OF EXPERIMENT

Two geometrically similar apparatus were used in the experimental program. A full-scale air test cell was built at Colorado State University, and an existing small-scale water cell at SERI was modified for the test program. An air test cell as shown in Figure 2 with sides 2.44 m (8 ft) long was constructed for the air measurements. A constant flux wall was constructed of eight electrical resistance heaters consisting of a graphite based heating element with a uniform resistance over the entire surface. The heaters were mounted on plywood sheets which are mounted to a stud wall. Aluminum foil was glued to the heater surfaces to provide a low emissivity ($\epsilon = .04$) surface for minimization of radiation exchange. A separately heated air gap on the exterior side of the hot wall was used to minimize direct losses from the heated wall to the environment. Each electrical resistance heater was powered by a variac which is connected to a voltage regulator. The current and voltage supplied to the heaters was measured with a calibrated voltammeter. The power supplied to the hot wall varied from 30 to 300 watts.

The constant temperature cold wall was constructed of copper solar collector absorber plates mounted on an insulated stud wall. Cold water entered a manifold at the bottom of the absorber plates, rose through 9 mm copper tubes 7.5 cm apart brazed to the absorber plate, and exited from an upper manifold. The water flow rate was maintained at a rate such that the difference between the inlet and outlet temperatures was no greater than 0.5 °C. The remaining four insulated surfaces were formed from insulated Celotex foam panels with an aluminum facing. They were insulated with 0.5 to 1 m thick fiberglass insulation. The partition that divided the test cell into two zones consisted of two layers of 2.5 cm thick aluminum Celotex panels that were erected parallel to the active walls. There was a 2.0 cm air gap between the Celotex panels. The ratio of the partition thickness to the enclosure height is 0.028.

The test cell was instrumented with 85 copper-constantan (Type T) thermocouples. Thermocouples measuring air temperatures were covered with radiation shields. Heat conduction through the test cell boundaries and across the partition was measured by thermocouples located on and within the test room walls, floor, ceiling, and partition. Thermocouples located near conducting surfaces were checked to insure that there were no ground loops. Temperature difference between zones and the stratification in each zone was determined by thermocouples suspended within each zone of the test cell and just outside the hot side of the partition aperture. An isothermal block was provided as a temperature reference for the test cell thermocouples. Thermocouple voltage measurements were made with an HP3497A data acquisition unit which configured for voltage to temperature conversion using software compensation. Data scanning of the HP3497A was controlled by a PC type computer. Software for data acquisition performed scans at regular intervals, converted raw voltage data to temperature, and stored temperature data on a floppy disk.

The external conduction heat losses from the test cell was measured by heating the cell with the cold wall water supply turned off. Measurements of the resulting conduction temperature profile in the six bounding surfaces were then used to determine empirical thermal conductivities for the heated wall, cooled wall, and the insulated side walls, ceiling and floor. The effective thermal conductivity of the dividing partition was measured with a full partition in place (Ap = 0) to eliminate interzonal convection, and with heat applied at the hot wall, and removed at the cold wall. The external and internal effective thermal conductivity were measured over a range of input power. For a flux Rayleigh number of 2×10^{12} and Ap = 0.1, the external heat loss was 15 percent of the supplied heater power, and the partition conduction 7 percent. For a smaller aperture of Ap = 0.01, the external heat loss was 22 percent, and the partition conduction 16 percent.

The air test cell required about 30 hours to reach steady state. The variation in the local heat flux on the hot wall was estimated to be about 7 percent, primarily due to different vertical temperature stratification profiles between the guard heater air gap and the hot wall. Average local temperature variations in the cold wall were about 5 percent of the wall to wall temperature difference. Transient cold wall fluctuations due to diurnal water temperature variation were negligible.

The interzonal radiation exchange was determined for each test point using a three-dimensional Monte Carlo method, MONT3D, developed by Burns and Maltby (1986) which calculated exchange factors between interior surfaces. The absorptivity of the Celotex aluminum surfaces of the heated and insulated walls was 0.04 ± 0.02, and the absorptivity of the black chrome cold wall was 0.11 ± .02, as measured by a Gier-Dunkle D9-100 infrared interferometer. The measured interior surface temperatures and absorptivities were used in conjunction with exchange factors for a given three-dimensional geometry to calculate the interzonal radiation exchange. For a flux Rayleigh number of 2×10^{12}, the net radiation heat transfer from the hot wall to the cold wall was 10 percent of the input power at an aperture ratio of 0.1, and 2 percent at an aperture ratio of 0.01. An energy balance was applied to each insulated interior surface to determine the convective heat transfer to the air from the difference between the net radiation and conduction heat transfer. In the hot zone the floor is irradiated by both the heated wall and the ceiling, resulting in a higher floor

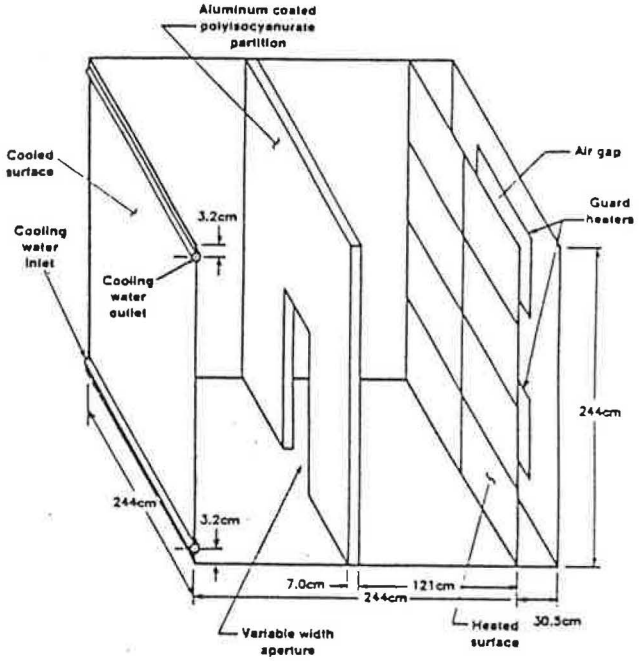

Figure 2. Air test cell.

temperature. The net convection to the air from the floor was 3 percent at Ap = 0.1, and 5 percent at Ap = 0.01, at the representative flux Rayleigh number. The net radiation heat transfer to the partition was 2 percent at Ap = 0.01.

An existing small-scale test cell at SERI was used for the water experiments. The water test cell was also of a cubic geometry with sides of length 0.57 m (2 ft). This apparatus is equipped with a constant flux hot wall, a constant temperature cold wall, and an insulating partition with an aperture of height H/2 and varying width. Since this is the same apparatus used by Scott (1986) most of the details relating to construction are already published and do not warrant repetition here. However, for experimental work presented in this study, there were modifications to this apparatus, as well as a complete recalibration and revised operating procedure.

The partition thermal conductivity was reduced by use of 2.54 cm (1 inch) thick polystyrene partitions coated with epoxy based paint and undercoated with latex paint. The partition thickness relative to the enclosure height was 0.044. The smaller apertures (Ap = .0031, .0051, .01) were formed from Plexiglas slots to increase the precision of the aperture geometry. The metal floor of the test cell was insulated from inside with neoprene rubber sheet to reduce floor conduction from the hot wall to the cold wall. The core temperature difference was measured using differential thermocouple wiring. The constant flux hot wall was not modified. The power supplied to the hot wall varied from 40 to 750 W. Since this apparatus was not equipped with a voltage regulator, there were variations in total flux due to hourly voltage fluctuations. When recording steady state points, transient fluctuations in flux were typically 4 percent of the total flux. Average local hot wall flux variations due to vertical conduction were 7 percent of the total flux. Average local temperature variations in the cold wall were typically 5 percent of wall to wall temperature difference. Hourly variations

in cooling water temperature were typically 3 percent of the wall to wall temperature difference. Recalibration of thermocouples and the fluxmeter yielded temperature measurement uncertainty of ± 0.14°C, and power measurement uncertainty of ± 2 percent. The differential thermocouples were calibrated to measure a temperature difference with an uncertainty of ± 0.03°C. The external heat loss was about 1 percent, and for an aperture ratio of Ap = 0.01, the partition conduction was about 5 percent of the input power.

For both enclosures, the amount of energy convected through the aperture was calculated from an energy balance on the hot zone. The energy convected was found from the difference between the power input to the variacs and the heat loss by conduction through the hot zone boundaries, heat conducted through the partition, and the interzonal radiation exchange. Further information is given in Neymark (1988). The fluid properties used in the calculations of dimensionless parameters were evaluated at the average of the area weighted average temperature of the cold wall and midpoint temperature of the hot wall. The reference temperature of the constant flux wall was its midpoint temperature. The effects of local relative humidity on air properties were found to be negligible. The Nusselt number is defined as

$$Nu = Q/Wk(T_H - T_c) \qquad (1)$$

and the flux Rayleigh number is defined as

$$Ra^* = g\beta H^4 q''/k\nu\alpha \qquad (2)$$

The flux Rayleigh number, Ra^*, is the product of the Rayleigh, Ra, and Nusselt numbers so that $Ra^* = 10^{12}$ corresponds to $Ra = 10^{10}$. A laminar boundary layer flux Rayleigh number exponent of 1/5 corresponds to a Rayleigh number exponent of 1/4. The temperature difference across the aperture was measured in the center of each zone at the aperture half height, and nondimensionalized by the wall to wall temperature difference:

$$\Delta T^* = \frac{T'_H - T'_c}{T_H - T_c} \qquad (3)$$

The parameter ΔT^* is a measure of the thermal resistance ($\Delta T/Q$) of the aperture relative to the total thermal resistance across the enclosure.

The uncertainties in the air cell Nu, Ra^*, and ΔT^* due to power and temperature measurement uncertainties have been estimated to vary from 4 to 11 percent, 5 to 11 percent, and 2 to 100 percent respectively, increasing as the aperture ratio increased. The uncertainties in the water cell Nu, Ra^*, and ΔT^* have been estimated to vary from 4 to 5 percent, 3 to 4 percent, and 2 to 50 percent. The error analysis was calculated at a confidence interval of 95 percent using standard random error analysis, Taylor (1982).

A hot wire anemometer and smoke flow visualization was used in the air cell for characterization of the flow field near the hot wall. Dye injection was used in the water cell for flow visualization.

The aperture ratio in the air cell ranged from 0.50 to 0.0045, and in the water cell from 0.50 to 0.0031. The aperture ratio in both cells was varied by changing the aperture width only, as the aperture height was held constant at h/H = 0.5. The flux Rayleigh number in the air cell ranged from 5×10^{11} to 5×10^{12}, and in the water cell from 4×10^{11} to 1×10^{13} The air cell Prandtl number was 0.7, and the water cell Prandtl number was approximately 6.

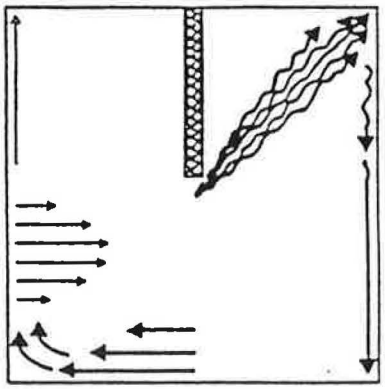

SIDE VIEW

Section which Includes Aperture

Figure 3. Flow visualization in water cell, Ap = .0051.

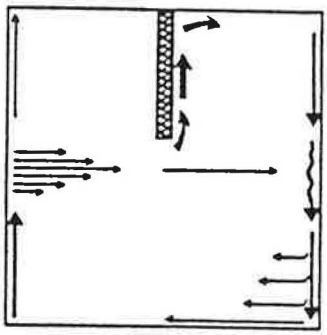

Figure 4. Flow visualization in water cell, Ap = 0.10.

RESULTS AND DISCUSSION

Flow visualization in the water test cell was performed at Ap = 0.0051 and at Ap = 0.10. The flux Rayleigh number was 2×10^{12}. The primary flow loop for Ap = 0.0051 is depicted in Figure 3. The upward boundary-layer flow along the hot wall was laminar. The hot wall boundary layer separated from the wall at $H/4 < y < H/2$. Before separation some waviness was visible in the boundary layer. The detrained boundary layer thickened and moved horizontally as shown. This horizontal flow accelerated as it moved through the aperture and exited the aperture in the form of a turbulent jet. The jet density fluctuations were visible without the assistance of injected die and were measured by a thermocouple traverse. The jet moved toward the cold wall at about a 45° angle with respect to the vertical axis indicating a relatively even balance between buoyancy and inertia in the jet. Along the cold wall, the flow was wavy laminar with small vortices along the edge of the boundary layer.

Flow visualization studies for the 0.10 aperture are depicted in Figure 4. Flow along the hot wall is characterized by a wavy laminar boundary layer. This boundary layer separated at $(3/8)H < y < (5/8)H$ and moved toward the aperture with a velocity profile as shown. After leaving the aperture and entering the cold zone, the flow rose as a laminar plume upward along the partition. The plume rose to the top of the

enclosure where it turned horizontally and thickened as it moved toward the cold wall. A small portion of cooler fluid entrained at the bottom of the horizontal boundary layer in the hot zone continued its horizontal path toward the cold wall after it exited the aperture. The cold wall boundary layer started out in a wavy laminar regime near the top of the enclosure (y = H) and grew more turbulent as it headed down toward where the secondary horizontal flow collided with this boundary layer. At y > H/2 the cold wall boundary layer turbulence begins to subside until wavy laminar flow is again attained.

Temperature measurements along the length of the active wall in the water-filled enclosure were made with a thermocouple probe, at distances 1.5 mm and 3 mm from the wall. The probe consisted of a 0.1 mm wire with a 0.5 mm junction. The wire behind the tip was encased in a glass tube to reduce probe conduction. The probe indicated no temperature fluctuations, consistent with the laminar wall flow observed with dye injection.

Flow visualization in the air cell was performed at Ap = 0.10, and Ra ≈ 2×10^{12} using isothermal smoke injection along the hot wall. The smoke particles were visible only for about 0.5 m. The boundary layer on the lower half of the hot wall appeared turbulent. The boundary layer was observed to separate from the hot wall at y = H/2, the aperture height. Figure 5 shows the hot wire output located vertically at y = H/4. Measurements were taken at 1.3 cm, 2.5 cm, and 5.1 cm outward from the wall. The velocity fluctuations at 1.3 and 2.5 cm are characteristic of turbulent flow in the boundary layer.

A comparison of air-filled and water-filled enclosure relative vertical temperature stratification as a function of Ap for Ra^* = 2×10^{12} is presented in Figures 6 and 7 for the hot zones and cold zones, respectively. The horizontal location of these data points are the midpoint between the partition and appropriate active wall along the length, and the midpoint between the sidewalls along the width. In these figures y/H is a dimensionless height where y is the height of the data point and H is the height of the test cell. The relative stratification, θ, is defined by

$$\theta = \frac{T_y - T_c}{T_{H/2} - T_c} \qquad (4)$$

where T_y is the temperature at the height y, T_c is the area weighted average cold wall temperature, and $T_{H/2}$ is the temperature at the midheight of the appropriate core.

In general, the air is less stratified than the water. In Figure 6, stratification in the lower quarter of the hot zone tends to increase slightly with decreasing AP, whereas stratification at midheight and above decreases with decreasing aperture. This is because the upper core acts as a heat source. Since the increased horizontal boundary layer activity at larger Ap causes more entrainment of the fluid above, there is more energy drawn from the upper region and the relative stratification is larger. In Figure 7 the water stratification in the upper half of the cold zone increases with decreasing aperture size. The relative air stratification is virtually unchanged.

The nondimensional horizontal stratification across the aperture ΔT^* is shown in Figure 8 for the air cell, and in Figure 9 for the water cell as a function of Ra^* and Ap. In general the stratification or temperature difference across the aperture increases

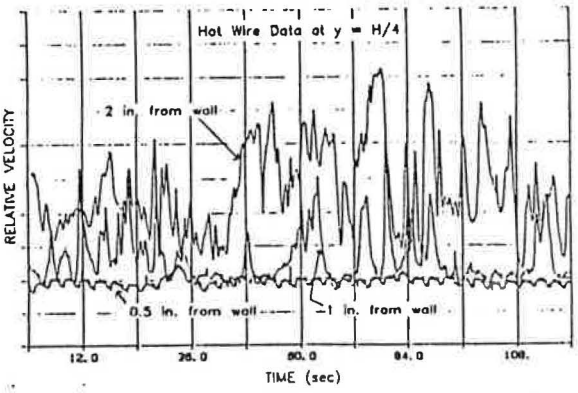

Figure 5. Velocity fluctuations in hot wall boundary layer in air cell.

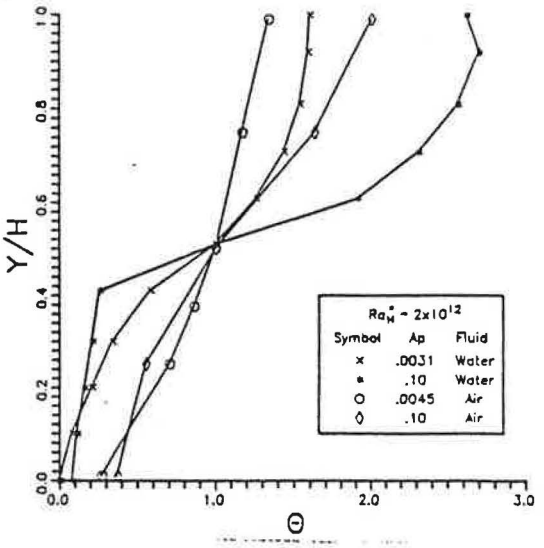

Figure 6. Vertical temperature stratification in hot zone at $Ra^* = 2 \times 10^{12}$.

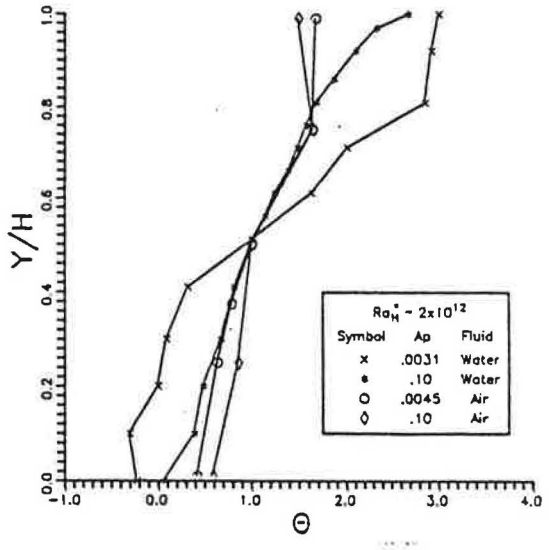

Figure 7. Vertical temperature stratification in cold zone at $Ra^* = 2 \times 10^{12}$.

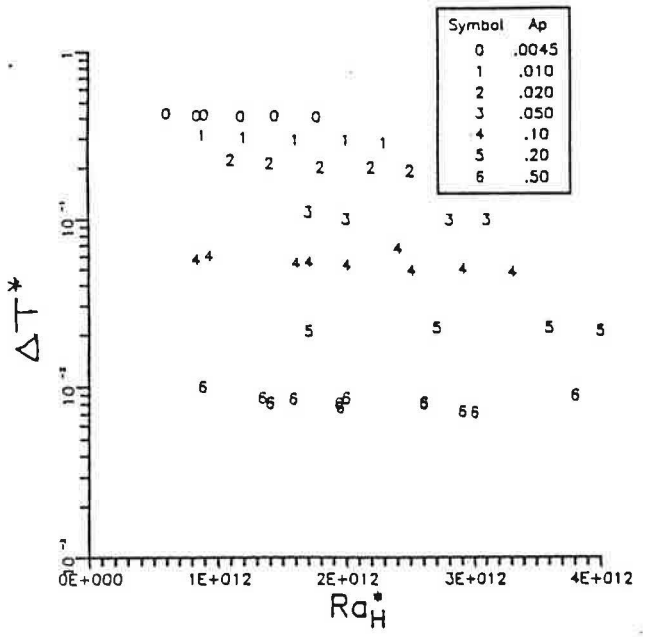

Figure 8. Horizontal temperature stratification in air.

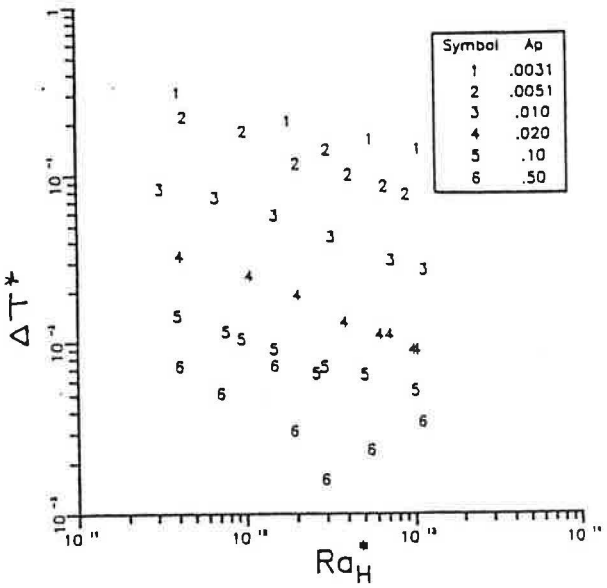

Figure 9. Horizontal temperature stratification in water.

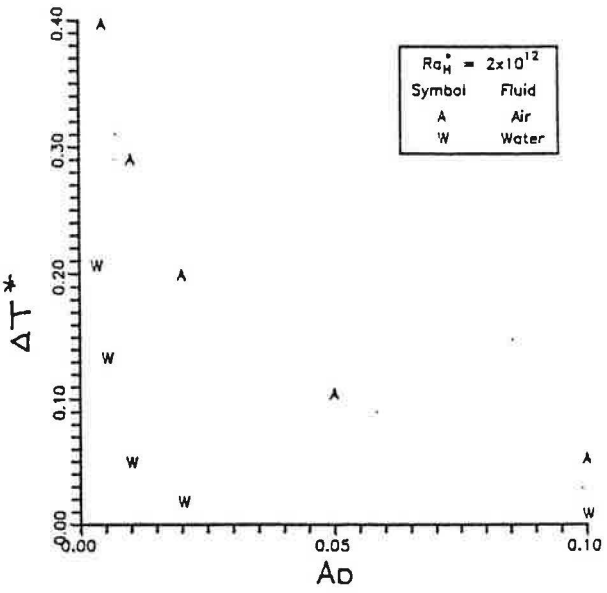

Figure 10. Comparison of air and water horizontal stratification.

with decreasing Ap and Ra^*. As the aperture ratio decreases, the counterflowing horizontally moving fluid layers have more interaction as they flow through the aperture opening. At some point, as the aperture ratio is decreased, the horizontal boundary layer flow becomes blocked, giving rise to a temperature gradient across the aperture.

The water stratification data is more sensitive than the air data to changes in the flux Rayleigh number. As Ra^* decreases, the wall boundary layer thickness increases, which will increase the thickness of the fluid layers moving through the aperture causing increased counterflow interaction at the aperture. The thickness of the laminar water boundary layer is a stronger function of the flux Rayleigh number than the thickness of the turbulent air boundary layer.

The stratification across the aperture for $Ra^* = 2 \times 10^{12}$ as a function of aperture size for both the water and air data is shown in Figure 10. As the aperture size is decreased, the air ΔT^* will begin to increase before the water ΔT^*, i.e., the minimum aperture size to prevent horizontal stratification is larger for air than water.

The air Nusselt number is plotted in Figure 11 as a function of flux Rayleigh number. A curve fit for each aperture using $Nu = a\,Ra^{*b}$ yields the a and b coefficients shown in Table 1. As the aperture ratio decreases from 0.50 to 0.0045, the Rayleigh number exponent increases from 0.296 to 0.426. The Nusselt number does not change significantly until Ap = 0.05, which is the same aperture ratio at which the temperature difference across the partition began to show a sharp increase.

The water Nusselt number is plotted in Figure 12, and the corresponding $Nu = a\,Ra^{*b}$ correlation coefficients for a particular aperture are shown in Table 2. As the aperture ratio is decreased from 0.50 to 0.0031, the Rayleigh number exponent increases from 0.192 to 0.289. If a critical aperture size is arbitrarily defined as a 10 percent reduction in the Nusselt number, interpolation between data points in Figure 12 indicates that the critical value of aperture size occurs at Ap = 0.025, which is about the same aperture ratio at which the temperature difference across the partition begins to increase. The air and water Nusselt numbers for $Ra^* = 2 \times 10^{12}$ are plotted versus aperture ratio in Figure 13. The air Nusselt number is about 15-30 percent higher than the water Nusselt number for aperture ratios larger than 0.01. This is a consequence of the turbulent hot wall boundary layer in the air cell, which has greater heat transfer than a laminar flow at the same Rayleigh number. Due to the difference in the flow regimes, a single $Nu - Ra^* - Pr - Ap$ equation was not developed for both the air and water data.

Table 1. Correlation Coefficients for Air Data
$(h/H = 0.5)\ Nu = a\ Ra^{*b}$

Ap	a	b
.50	0.0202	0.296
.20	0.0356	0.276
.10	0.0201	0.295
.05	0.0404	0.270
.02	0.0139	0.303
.01	0.00332	0.348
.0045	0.000294	0.426

Table 2. Correlation Coefficients for Water Data
$(h/H = 0.5)\ Nu = a\ Ra^{*b}$

Ap	a	b
.50	0.285	0.192
.10	0.297	0.189
.02	0.209	0.198
.01	0.0483	0.247
.0051	0.0468	0.246
.0031	0.0111	0.289

The simultaneous onset of aperture ratio dependence for the Nusselt number and the horizontal stratification across the aperture indicate a change in the flow regime from a dominant boundary layer regime to a blocked flow bulk density driven regime. In the boundary layer regime, the resistance to heat transfer across the enclosure is in the boundary layers on the heated and cooled walls, and the thermal resistance of the aperture is negligible. In the blocked flow regime, the thermal resistance at the aperture is at least the same magnitude as the thermal resistance at the walls, so that the enclosure heat transfer is dependent on the aperture size.

Differences in behavior of air and water data documented in this section are due to the different boundary layer flow regimes along the hot wall in the two enclosures. The turbulent air boundary layer is thicker than a corresponding laminar water boundary layer. When this boundary layer detrains from the hot wall further enlargement is expected due to turbulent mixing. The resulting horizontal boundary layer is then more easily blocked by the partition and also mixes better with the core which creates a situation that is more representative of a bulk density dominated transport regime. Since boundary layer flows in the water experiments are laminar, the boundary layer in the water-filled enclosure results in the onset of flow blockage at a relatively smaller aperture.

The water data correlation is compared to previous aperture experiment correlations in Figure 14 on a log-log plot. All equations on this plot are for h/H = 0.5. The correlations from Scott et al. (1986) are shown for Ap = 0.0026 and 0.5. The Scott line is slightly higher due to the thermal conductance of the aluminum floor of his test cell which was insulated in the present series of experiments. The constant temperature hot wall Nusselt-Rayleigh number equation of Nansteel and Greif (1984) was transformed into a Nusselt-flux Rayleigh number equation. The constant flux hot wall equations are lower than the constant temperature hot wall equation, due to the characteristic hot wall temperature assumed for the constant flux experiments. This temperature was chosen to be the midheight temperature. However, the boundary layer heat transfer along the hot wall occurs on the lower half, as the boundary layer separates when it reaches the top of the aperture. Therefore, the characteristic temperature driving the hot wall boundary layer is actually the wall temperature at y = H/4, half of the aperture height. This temperature is less than the wall temperature at h = H/2, so a Nusselt number calculated with a hot wall temperature at y = H/4 would be greater than one calculated with a hot wall temperature at y = H/2.

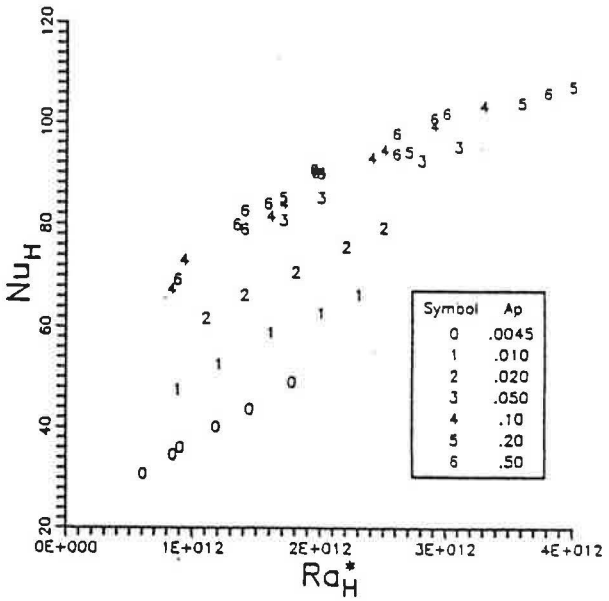

Figure 11. Nusselt vs. flux Rayleigh air data.

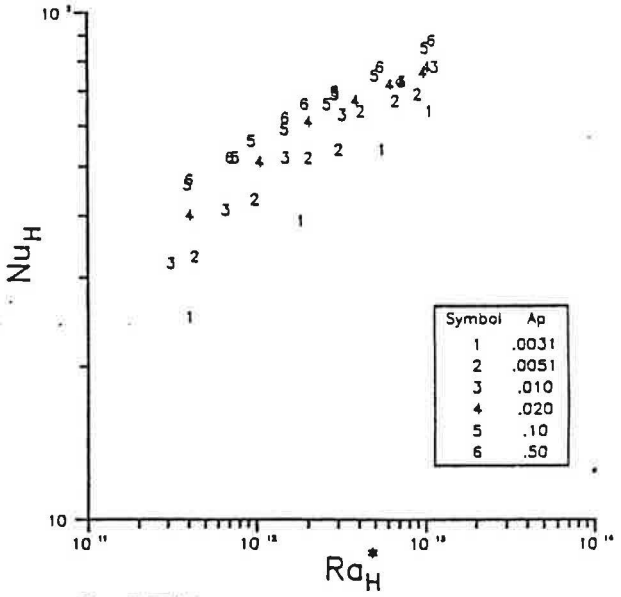

Figure 12. Nusselt vs. flux Rayleigh water data.

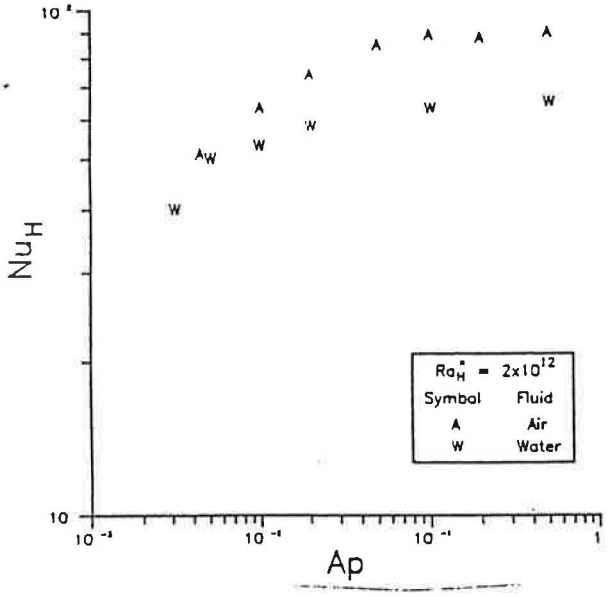

Figure 13. Nusselt vs. aperture ratio for air and water at $Ra_H^* = 2 \times 10^{12}$.

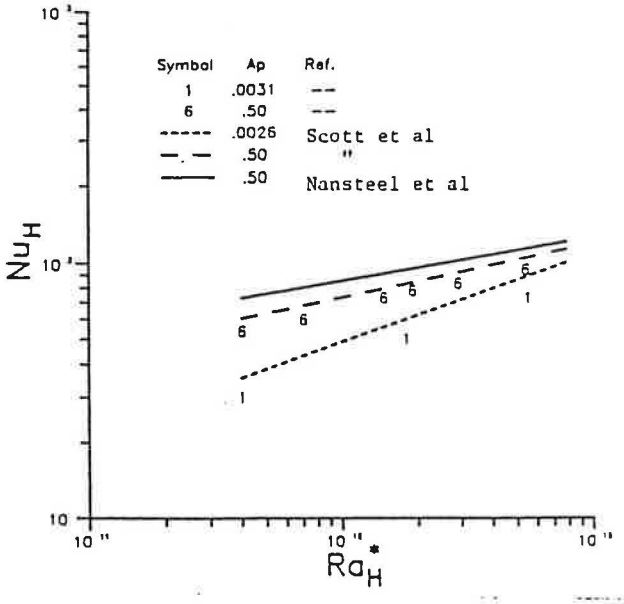

Figure 14. Comparison of water data to previous results.

SUMMARY AND CONCLUSIONS

Specific conclusions can be drawn concerning the effects of aperture and flux Rayleigh number on interzonal natural convection in water and air. Studies of the effect of variable aperture width at constant Ra_H^* show that as aperture size decreases the flow regime transitions from a boundary layer to a bulk density dominated transport mechanism. The data shows little change in Nusselt number with varying aperture width for $Ap > 0.04$ in air and $Ap > 0.02$ in water. Below these critical values of Ap, the Nusselt number becomes a strong function of Ap, and the horizontal stratification across the aperture approaches the overall enclosure temperature difference.

At $Ra_H^* = 2 \times 10^{12}$, the boundary layer along the lower half of the hot wall is laminar in the water-filled enclosure, while in the air-filled enclosure this boundary layer exhibits velocity fluctuations which are characteristic of turbulent flow. The turbulent hot wall boundary layer results in larger Nusselt numbers and the onset of boundary layer flow blockage at larger apertures in air-filled enclosures when compared to water-filled enclosures.

ACKNOWLEDGMENTS

This work was supported by the Department of Energy, the Solar Energy Research Institute, and the Associated Western Universities.

REFERENCES

Anderson, R., and Kreith, F., 1987, "Natural Convection in Active and Passive Solar Thermal Systems," Advances in Heat Transfer, Vol. 18, pp. 1-86.

Brown, W. G., and Solvason, K. R., 1962, "Natural Convection through Rectangular Openings in Partitions 1," Int. J. Heat Mass Transfer, Vol. 5, pp. 859-868.

Burns, P., and Maltby, J., 1986, "MONTE User's Manual for MONT2D and MONT3D," Department of Mechanical Engineering, Colorado State University, Fort Collins, CO.

Cheesewright, R., and Zial, S., 1986, "Distributions of Temperature and Local Heat Transfer Rate in Turbulent Natural Convection in a Large Rectangular Cavity," Proc. 8th Int. Heat Transfer Conf., Vol. 4, pp. 1465-1470.

Lin, N. N., and Bejan, A., 1983, "Natural Convection in a Partially Divided Enclosure," Int. J. Heat Mass Transfer, Vol. 26, pp. 1867-1878.

Nansteel, M. W., and Greif, R., 1984, "An Investigation of Natural Convection in Enclosures with Two and Three Dimensional Partitions," Int. J. Heat Mass Transfer, Vol. 27, pp. 561-571.

Neymark, J., 1988, "Aperture and Prandtl Number Effect on Interzonal Natural Convection," M.S. Thesis, Colorado State University, Fort Collins, CO.

Olson, D. A., Glicksman, L. R., and Ferm, H. M., 1986, "Scale Model Studies of Natural Convection in Enclosures with Turbulent Vertical Boundary Layers," ASME Winter Annual Meeting, Anaheim, CA.

Scott, D., Anderson, R., and Figliola, R., 1986, "Blockage of Natural Convection Boundary Layer Flow in a Multizone Enclosure, AIAA/ASME Hat Transfer and Thermophysics Conference, Boston, MA.

Taylor, J. R., "An Introduction to Error Analysis, 1982, " University Science Books, Mill Valley, CA.